Journal of Renewable Materials

Tech Science Press

DOI: 10.32604/jrm.2022.022501

ARTICLE

Study on the Hydration and Physical Properties of Cement by M18 Polycarboxylate Superplasticizer Modified Graphene Oxide

Dalong Liao, Dongxu Li*, Shun Zhou, Xiaotao Zhang and Ying Fang*

College of Materials Science and Engineering, Nanjing Tech University, Nanjing, 211816, China

*Corresponding Authors: Dongxu Li. Email: dongxuli@njtech.edu.cn; Ying Fang. Email: powderfang@163.com

Received: 13 March 2022 Accepted: 13 April 2022

ABSTRACT

Graphene oxide (GO) as a new nano-enhancer in cement-based materials has gained wide attention. However, GO is easy to aggregate in alkaline cement mortar with poor dispersibility. This hinders its application in practical infrastructure construction. In this work, GO-M18 polycarboxylate compound superplasticizer (GM) were obtained by compounding the M18 polycarboxylate superplasticizer with GO solution at different mass ratios. The dispersion of GM in alkaline solution was systematically studied. The phases and functional groups of GM were characterized by XRD and FTIR. The effects of GM on the cement mortar hydration and the formation of microstructure were investigated by measuring the heat of hydration, MIP, TG/DSC, and SEM. The results show that the long-chain structure of the M18 polycarboxylate superplasticizer can increase the interlayer spacing of GO and weaken the force between GO sheets. The modified GO can be uniformly dispersed in the cement slurry. GM can accelerate the early hydration process of cement, which can increase the content of $Ca(OH)_2$ and decrease the grain size. It can optimize the pore size distribution of cement-based materials, increase the density of harmless and less harmful pores, thereby improving mechanical properties. Such methods can transform traditional cement-based materials into stronger, more durable composites, which prolong the life of cement-based materials and reduce the amount of cement used for later maintenance. This provides an idea for achieving sustainability goals in civil engineering.

KEYWORDS

Modified graphene oxide; cement; polycarboxylate superplasticizer; hydration properties; me-chanical performance

1 Introduction

Concrete is an artificial stone formed by mixing, molding, hardening, and curing. It contains cement as the main cementing material, which is mixed with sand and gravel, in addition to mineral admixtures, water, and additives. But typical concrete is a brittle material with poor crack resistance, low tensile strength, and strain capacity. In the course of long-term service, the serviceability of concrete is greatly reduced by temperature, humidity, various salts, water, and loads. With the continuous progress of modern materials science and technology, the rapid development and breakthrough of nanomaterials provide an effective approach to improve the working properties of cement-based materials at the microscopic scale [1,2]. Nanomaterials modified cementitious materials can effectively improve the mechanical strength and durability performance in harsh environments, transforming traditional cementitious materials into

stronger, smarter and more durable composite materials [3,4]. In addition, it helps to limit the leaching of calcium hydroxide ($Ca(OH)_2$), which is responsible for most of the deterioration of concrete. This prolongs the service life of concrete, decreases service and maintenance costs, and effectively reduces the amount of cement used within a certain period of time [5,6]. Therefore, it can reduce the energy consumption and CO_2 emissions in the cement production process, which can help protect the environment and thus promote the sustainable development of the global construction industry.

Nanomaterials offer a considerable impact on the performance of cementitious materials. Firstly, their smaller particle size can fill the voids inside the cement, which can enhance the density of the cement with improved strength [7]. Secondly, nanomaterials have high specific surface energy and high chemical activity, which can influence the hydration process of cement. Nanomaterials, such as nano-alumina and nano-silica, can undergo a secondary hydration reaction with calcium hydroxide ($Ca(OH)_2$) formed in the cement hydration, which generates a dense calcium silicate hydrated (C–S–H) gel that improves the strength of cement-based materials [8,9]. Finally, nanomaterials have many active bonds on their surfaces and can help to facilitate crystal nucleation. During the hydration of the cement, the hydration products are generated around the nuclei on the surface of nanomaterials, turning the originally loose C–S–H gel into a denser network structure. Graphene oxide (GO) is a lamellar nanomaterial with a large specific surface area and abundant functional groups, such as hydroxyl (–OH), carboxyl (–COOH), epoxy (–C–O–C–), etc. It not only weakens the van der Waals forces between the graphene sheets with the increased electrostatic repulsion to enable stable dispersion in water but also promotes interaction with other media through the chemical activity of GO [10,11]. The data shows that GO provides additional dimensions to cement and cement-based materials, which can substantially improve the potential of optimizing the microstructure and improving the macroscopic properties of the cement-based composites [12,13]. The development of GO as a nano-reinforcer to modify the properties of cementitious materials has become a new research hotspot [14–16].

GO is easily agglomerated in alkaline cement slurry and is difficult to disperse. When the GO dosing reaches a certain ratio, the uneven dispersion of the GO nanosheets in the cement slurry can cause a series of problems, such as microcracks, local defects, and increased pore structure, which leads to a decrease in the strength and workability of cement [17–19]. Therefore, it is important to develop homogeneously dispersed GO additives in cement-based materials. Many physicochemical methods have been used to disperse nano-materials, such as mechanical sonication, the addition of surfactants, and chemical functionalization [20,21]. Among them, ultrasonic dispersion is the most commonly used method, which can improve the GO dispersion to some extent. However, the ultrasonic process may disrupt the GO molecular structure and make smaller GO nanosheets. On the other hand, the direct addition of surfactant is a convenient and effective method to disperse GO in cement slurry solution. Yavari et al. [22] modified the graphene oxide surface with γ-MPS silane and significantly improved the dispersion of the modified graphene oxide in the resin. Modified graphene oxide was also used to improve the stability of cobalt complexes and reduce the activation energy in the redox decomposition region in the matrix. Zhang et al. [23] used KH550 to modify graphene oxide and found an optimal modification temperature of 60°C. Pooneh et al. [24] modified GO with 3-propyl isocyanate (TEPIC) to activate the surface functional groups of GO by improving the interfacial interaction between GO and polymer chains.

As a concrete water reducing agent, polycarboxylate superplasticizer is a typical polymeric surfactant. Its molecular chain contains –COOH, $–SO_3H$, –OH, polyoxyalkenyl links (–PEO–PPO), and –COO– and other reactive functional groups. These functional groups can provide anchoring, solubilization, electrostatic repulsion, and spatial site resistance repulsion, which involve strong adsorption and dispersion to the cement particles [25]. It has infinite structure and performance design space. Various polycarboxylate superplasticizers can be produced with different properties and characteristics by changing the types,

proportions, and reaction conditions of polymerized monomers [26]. Compared with other water-reducing agents, a polycarboxylate superplasticizer with good dispersion requires a lower dosage but offers a higher water reduction rate. Adding to concrete can reduce the slump loss with good volume stability and suitable different types of cement. Therefore, polycarboxylate superplasticizer has become one of the most used and actively researched water-reducing agents in domestic and international projects.

To make GO uniformly and stably diffused in the cement slurry solution, the excellent properties of GO are fully utilized. In this study, the thermally blending method was used to innovatively compound GO with M18 polycarboxylate superplasticizer at different mass ratio to obtain GO-M18 polycarboxylate compound superplasticizer (GM). GO nanoparticles were successfully dispersed in cement matrix by direct polymerization of GO with polycarboxylate superplasticizer. This method reduces the additional dispersant carrier and operation process, and improves the possibility of GO application in practical engineering. Furthermore, the effect of the GO content in GM compounds on the workability, hydration properties, pore structure, mechanical properties of cement, and the associated mechanism were investigated.

2 Materials and Methods

2.1 Materials

In this experiment, the solution concentration of graphene oxide (GO) was 7.5 g/L, provided by the School of Chemical Engineering, Nanjing University of Technology. The thickness of GO sheet layer is 0.8 nm. The polycarboxylate superplasticizer used in the compounding is M18 polycarboxylate superplasticizer (M18) provided by China Railway Aolite. It is a light yellow liquid with a solid content of 49.85%. Its transmission electron micrograph (TEM) is shown in Fig. 1, where GO is distributed in layers and there are multiple overlapping layers. The cement meets the requirements of PII 52.5N, which is made by Jiangnan Onoda Cement Company Limited (Nanjing, China). Table 1 illustrates the chemical composition of cement by XRF testing. The sand used in the experiment is ISO standard sand produced by Xiamen ISO standard sand Co., Ltd. (China), which meets the requirements of GB/T 17671–1999. The apparent density of sand is 2650 kg/m^3, the bulk density is 1810 kg/m^3, and the particle size range is 0.5–1.0 mm.

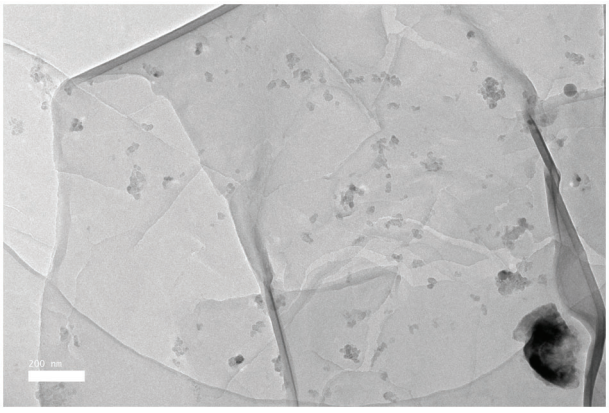

Figure 1: TEM diagram of GO

Table 1: Chemical compositions of cement (wt.%)

Composition	Percentage/%
SiO_2	21.45
Al_2O_3	4.33
Fe_2O_3	3.41
CaO	63.46
MgO	1.49
Na_2O	0.26
K_2O	0.57
TiO_2	0.24
MnO	0.14
P_2O_5	0.16
LOI	2.90

2.2 Methods

2.2.1 Preparation of GM Compound Superplasticizer

As shown in Table 2, the GM polycarboxylate compound superplasticizer was prepared by weighing M18 polycarboxylate superplasticizer and GO solutions in the mass ratio of 100:40 (GM-1), 100:80 (GM-2) and 100:100 (GM-3), respectively. Then, the M18 and GO solution were added to the three-necked flask, heated to 45°C in a water bath, and stirred continuously for 8 h with a mixer at a rate of 500 r/min. After cooling, the GM polycarboxylate compound superplasticizer was obtained.

Table 2: Mix ratio M18 and GO in GM compound superplasticizer

	M18-0	GM-1	GM-2	GM-3
M18:GO	100:0	100:40	100:80	100:100

2.2.2 Preparation of Cement Mortar

In this study, M18/cement (M18-0) cement mortar samples and GM/cement (denoted GM-1, GM-2, and GM-3, respectively) cement mortar samples were prepared. The water/cement is 29:100 (w/c = 0.29). The GM solid content was 0.1% of the cement mass (the solid content of M18-0, GM-1, GM-2 and GM-3 were 49.85%, 36.23%, 28.24% and 25.65%, respectively). The GM compound superplasticizer was first mixed with water and added to the mixing pot after 0.5 h of ultrasonic dispersion. To prepare the cement mixture, a JJ-5 planetary mixer was used. After the initial low speed mixing for 2 min, the mixing was paused for the 30 s followed by high speed mixing for 2 min. The sample was formed by vibration forming on a vibration table. After settling for 24 h, the sample was taken out from the mold. A series of tests were conducted after curing for 3, 7, and 28 d in a standard curing room (20°C/RH ≥ 95%).

2.2.3 Characterization

The chemical structures of the GM complexes were characterized by FTIR using the KBr tablet approach, where freeze-dried GM complexes and KBr powder were ground into a powdered mixture before being pressed into a disc. The phase composition of GM complex powder specimens was determined by the XRD. The main peak of $Ca(OH)_2$ [0 0 1] crystalline surface is near 18°(2θ), and the

information of the characteristic peak of $Ca(OH)_2$ [0 0 1] crystalline surface is analyzed by Jade software, and then the grain size is calculated according to Scherrer formula:

$$D = \frac{K\lambda}{B\cos\theta} \tag{1}$$

where D is the grain size (nm); K = 0.89, which is the Scherrer constant; λ is the wavelength of the X-ray, λ = 0.155 nm; B is the half-peak width of the diffraction peak (rad); and θ is the Bragg diffraction angle (rad).

A Saturated $Ca(OH)_2$ solution was chosen to simulate the alkaline environment in the cement slurry to observe the dispersion of the modified GO [27,28]. The blank sample was formed with 0.08 g of GO solution and 30 g of saturated $Ca(OH)_2$ solution without the addition of a modifier. For the experimental sample, 0.45 g GM-2 complex solution was added to 35 g saturated $Ca(OH)_2$ solution. The mixture was stirred and left to stand. The dispersive observation test was carried out after mixing GO and GM in the saturated $Ca(OH)_2$ solution for 0.5 h. The fluidity of cement mortar was measured based on the Chinese national standard GB/T 8077-2000 "Test method for homogeneity of concrete admixtures". The truncated cone die used for the test has an upper opening diameter of 36 mm, a lower opening diameter of 60 mm, and a height of 60 mm. The setting time of neat cement slurry at the same water consumption was tested by a Vicat apparatus. When the test needle sinks to 4 mm from the bottom plate, it is the initial setting time. When the test needle sinks into 0.5 mm, and the trace formed by the ring attachment disappeared, the final setting time is recorded. The mechanical properties of the four groups of specimens at 3 and 28 d were tested with a strength testing machine. The specific test procedure follows the Chinese national standard GB/T 17671-1999 "Test method of cemented sand strength". The early hydration rate and cumulative heat release of cement samples were measured by an eight-channel TAM air isothermal calorimeter using internal mixing method. The test sample contains 4 g cement and 1.8 g water (w/c = 0.45). The sample testing time is 72 h and the temperature is 20°C. TG/DSC was used to investigate the hydration products and the degree of hydration. After drying at 50°C for 24 h, the samples were pulverized and ground into powder. During the test, the temperature was heated from 20°C to 1200°C at a rate of 10 °C/min. The heating process was protected by nitrogen. The following equation was used to calculate the $Ca(OH)_2$ content after the completion of the test and was used to calculate the hydration rate of cement [29,30]:

$$Ca(OH)_2 \xrightarrow{400^\circ - 500^\circ C} CaO + H_2O \uparrow \tag{2}$$

$$CaCO_3 \xrightarrow{680^\circ - 740^\circ C} CaO + CO_2 \uparrow \tag{3}$$

$$m_{Ca(OH)_2}(\%) = \frac{M_{Ca(OH)_2} \times m_{H_2O}}{M_{H_2O}} + \frac{M_{Ca(OH)_2} \times m_{CO_2}}{M_{CO_2}} \tag{4}$$

In the above equation, m_{H_2O} and m_{CO_2} represent the mass loss of $Ca(OH)_2$ and $CaCO_3$ when decomposed by heating, respectively, in percentage. $M_{Ca(OH)_2}$, M_{H_2O} and M_{CO_2} are the molecular weights of $Ca(OH)_2$, H_2O and CO_2, respectively.

The mercury intrusion porosimetry (MIP) and scanning electron microscope (SEM) were used for characterizing the microscopic pore structure of the cement specimen. After curing the samples for 3 and 28 d, the hardened cement samples were crushed to 3–5 mm. The samples were soaked in anhydrous ethanol for 24 h to terminate the hydration followed by drying in a blast drying oven at 50°C for 24 h. The microstructure of the samples was visualized by using an SEM. The cement specimens were processed into thin sheets and dried for microscopic morphological analysis. To enhance the electrical conductivity, a conductive carbon tape was used to attach the specimen to the sample holder, which was coated with a gold film using the magnetron sputtering method.

3 Results and Discussion

3.1 Chemical Structure Characterization of GM Compound Superplasticizer

Fig. 2 shows the FTIR spectra of GO, M18-0 and GM-2. The spectrum shows that there are many active functional groups on the surface of GO. For example, the two diffraction peaks at 3440 and 1640 cm^{-1} are the absorption peak of –OH and the stretching vibration peak of C=C, the stretching vibration peak of C=O and the vibrational absorption peaks of C–O–C correspond to the diffraction peaks at 1720 and 1110 cm^{-1}, respectively. The existence of these reactive functional groups provides a prerequisite for the coupling of GO and polycarboxylate superplasticizer. After compounding with the M18 polycarboxylate superplasticizer, the peaks associated with GM-2 remained the same, but the peaks related to $–CH_3$ (2886 cm^{-1}) and C–O–C (1342 cm^{-1}, 1110 cm^{-1}) became stronger. This suggests that the coupling of GO and M18 polycarboxylate superplasticizer did not change the main functional group species, and the interactions between the functional groups were mainly the hydrogen bonds as the intermolecular forces.

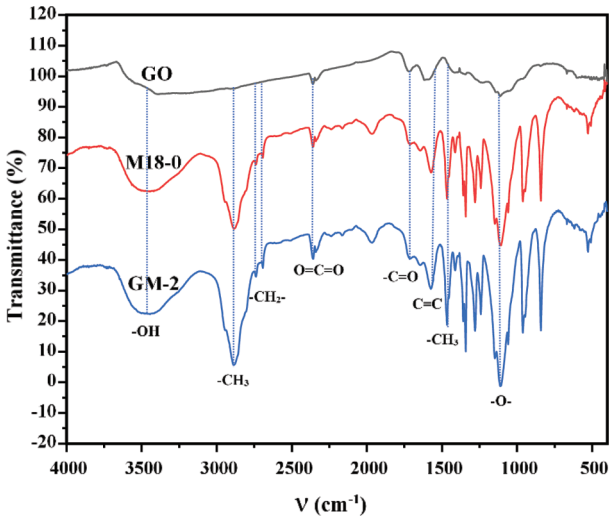

Figure 2: FTIR spectra of GO, M18-0 and GM-2

The XRD diffraction patterns of GO, M18-0 and GM-2 components are shown in Fig. 3. The GO particles were present as nanosheets with a characteristic diffraction peak near 11.3°. However, this peak was not observed from the GM-2 sample. This indicates that the GO lamellae were peeled off or disordered after the M18 polycarboxylate superplasticizer was compounded with GO. This is due to that during the drying process, the long side chains of the M18 polycarboxylate superplasticizer prevented the GO from approaching each other to form the order structure, resulting in the disordered stacking of uniformly dispersed GO lamellae.

3.2 Dispersibility of GM Compound Superplasticizer

Fig. 4a shows the dispersion of GO in water, Figs. 4b and 4c show the dispersion of GO, GM-2 in saturated $Ca(OH)_2$ solution. Due to the presence of functional groups containing oxygen, such as –OH, –COOH, C–O–C, and $–SO_3H$ on the surface of GO, it has good hydrophilicity, which is essential for good dispersion in aqueous solutions. Adding drops of GO aqueous solution to the saturated $Ca(OH)_2$ solution immediately caused agglomeration, which resulted in precipitation and stratification when left to stand [31]. This is due to the high pH value of the saturated $Ca(OH)_2$ solutions caused fast deprotonating of the –COOH forming more –COO–. The large amounts of Ca^{2+} coupled with the –COO– on the individual GO sheet to form the $–COO–Ca^{2+}–COO–$, leading to the self-agglomeration of GO sheets.

More importantly, the –COO– between two GO lamellae can also be coupled by Ca^{2+} bridging to form the –COO–Ca^{2+}–COO–, contributing to the mutual agglomeration between the GO lamellae [32]. This interlamellar complexation continuously extended, causing GO to agglomerate in the cement slurry solution. This is the main reason for the precipitation and delamination of GO. The agglomerated GO was unevenly dispersed in the cement mortar, which tends to form defects and weak areas in the cement matrix. This weakens the performance of cementitious materials. After the co-blending modification, the spatial site-blocking effect of the long side chains of M18 polycarboxylate superplasticizer hinders the agglomeration between the GO layers. GM-2 can be uniformly dispersed in the saturated $Ca(OH)_2$ solution.

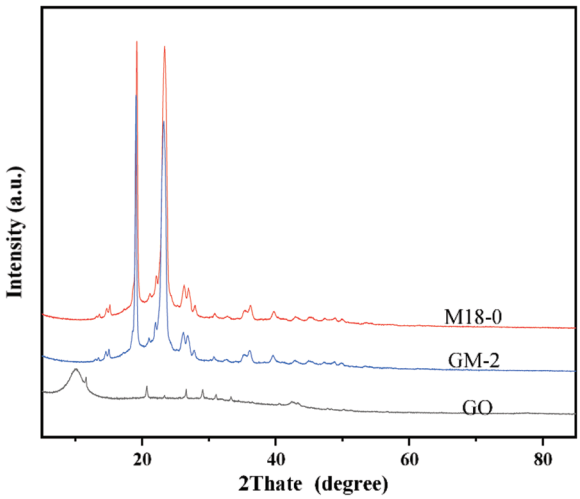

Figure 3: XRD patterns of GO, M18-0 and GM-2

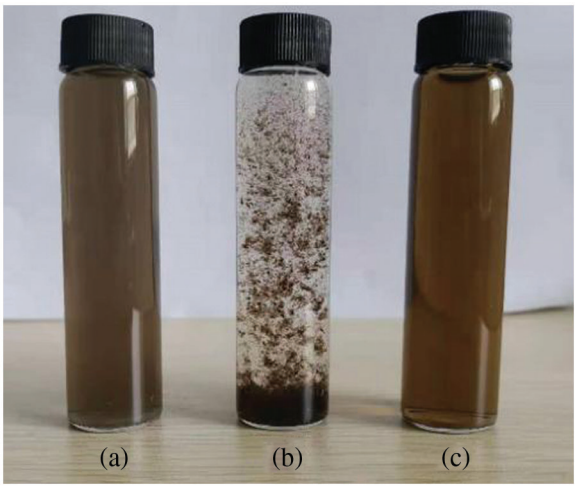

Figure 4: Changes in dispersion of GO/GM: (a) GO+H_2O; (b) GO + saturated $Ca(OH)_2$ solution; (c) GM+ saturated $Ca(OH)_2$ solution

3.3 Effect of GM on the Working Performance of Cementitious Materials

The fluidity, initial setting time, and final setting time of cement slurry for the M18-0 group and GM experiment groups are given in Table 3. Compared with the M18-0 group, the fluidity values of GM-1, GM-2 and GM-3 were reduced by 34, 50, and 59 mm, respectively. The corresponding initial setting time

was reduced by 9, 24, and 32 min, while the final setting time was reduced by 17, 26, and 38 min, respectively. This is because not only the GO surface contains a large number of active hydrophilic groups, such as –OH, –COOH and C–O–C, and GO itself, but also GO itself has the ultra-micro-size effect of nanomaterials. The GO has an extremely large specific surface area, capable of adsorbing a large amount of water [33]. After GO was compounded with M18 polycarboxylate superplasticizer, it can be uniformly dispersed in water, which reduces the quantity of free water and increases the friction between cement particles. The fluidity of GM was reduced, and with the increase of GO content, the fluidity decreased more. The shortening of the setting time indicates that GO promotes cement hydration.

Table 3: Effect of GM on the working properties of cement slurry

Sample	Fluidity (mm)	Setting time (min)	
		Initial	Final
M18-0	206	202	240
GM-1	172	193	223
GM-2	156	178	214
GM-3	147	170	202

3.4 Effect of GM on the Hydration Characteristics of Cement-Based Materials

3.4.1 Heat of Hydration

Fig. 5 shows the hydration heat release rate and cumulative heat release curve of cement. The behavior of hydration rate of each group is similar to that of ordinary silicates, which can be classified into five phases: (I) pre-induction; (II) induction; (III) acceleration; (IV) deceleration; and (V) stabilization [34]. The measured rate shows that the exothermic hydration in the GM component is significantly faster than that in the M18-0 group, with the fastest hydration rate was observed from the GM-1. For the heat release cumulated for 72 h, the GM-1 and GM-2 groups had higher values than that of the M18-0 group, while the GM-3 group had the lowest heat release. In the pre-hydration induction phase, the cement clinker dissolved. With the C_3A being the first to hydrate, ettringite (AFt) was rapidly formed and the first exothermic peak occurred. Since the GO in GM compound superplasticizer can be uniformly dispersed in the cement, resulting in the reduction of free water and delaying the hydration reaction. This, the exothermic peak of the GM component was delayed. With the increase of the GO content, the delaying becomes more significant. Meanwhile, the –COO– functional groups on the GO binds with Ca^{2+}, which reduces the free Ca^{2+} in the cement mortar with an accelerated C_3S reaction. Hence, the exothermic peak from the GM component is higher than that from the M18-0 group. However, when the GO dosing is too high, the excessive water adsorbed by GO also hinders the exothermic hydration reaction of the cement. Thus, the exothermic peak from the GM-3 group is lower than that from the GM-1 and GM-2 groups. During the accelerated and decelerated phases of cement hydration, the reaction process is accelerated and C_3S undergoes rapid hydration to form the hydration products of C–S–H gel and $Ca(OH)_2$ to establish a second exothermic peak. The reason is that as a nanomaterial, The high specific surface area and rich active functional groups of GO can effectively reduce the nucleation potential, provide nucleation sites for the hydration products and facilitate the crystallization and precipitation of $Ca(OH)_2$. It speeds up the hydration of the cement clinker and increases the early hydration heat release of the cement [35].

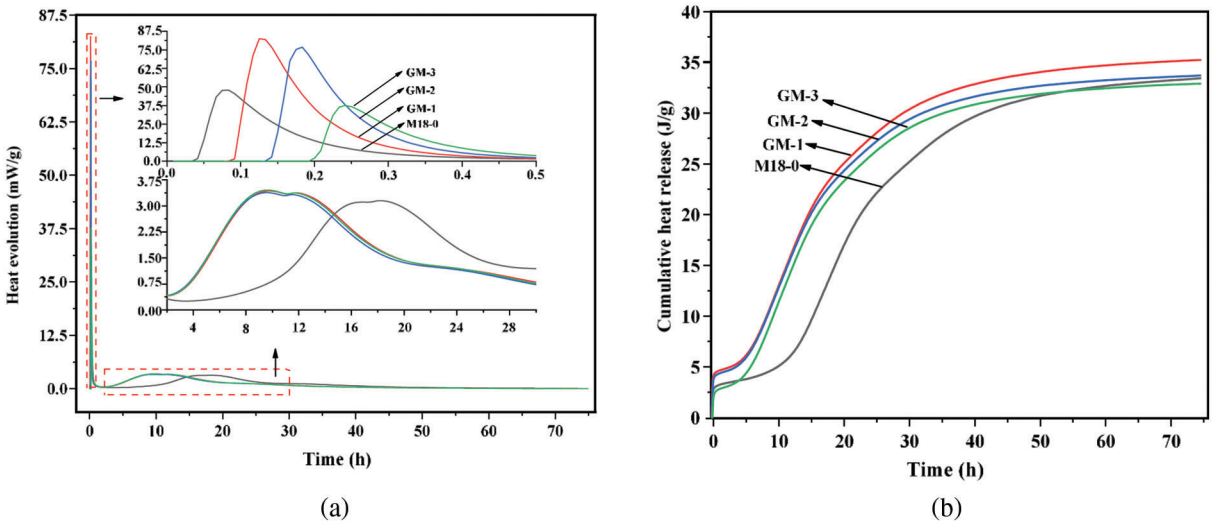

(a) (b)

Figure 5: The effect of GM on hydration heat of the cement. (a) The heat releases rate; (b) Cumulative heat releases

3.4.2 XRD

The effect of GM on the cement hydration was studied by comparing the differences in the types of hydration products and the $Ca(OH)_2$ content in each group of specimens. XRD measurements were carried out on the cement slurry samples. Fig. 6 shows the XRD pattern of the GM-cement sample, while Fig. 7 shows the change of the crystallite size of the $Ca(OH)_2$ along the [0 0 1] crystal plane. From Fig. 6, the GM did not change the composition of the physical phase of the specimen without new diffraction peaks. It means that GM does not directly participate in the hydration reaction of cement to form new hydration products. By analyzing the crystallite size of the hydration product of the $Ca(OH)_2$, it was found that the crystallite size from the GM-1 and GM-2 groups was lower than that of the M18-0 sample. This is because the active functional group of –COO– on the GO sheets acts as a nucleus center to bind the Ca^{2+} by forming the COO–Ca^{2+}–COO– aggregates, which facilitates the nucleation of $Ca(OH)_2$ crystals. However, GO does not directly act as one of the cement hydration reactants and ultimately does not change the $Ca(OH)_2$ content, so the $Ca(OH)_2$ grain size is reduced, and this effect is more pronounced after 3 d aging.

3.4.3 TG-DSC

Fig. 8 shows the thermogravimetric curves of M18-0, GM-1, GM-2 and GM-3 samples after curing for 3 d and 28 d. According to the TG curve, three weight loss peaks appeared in each group of samples. The low-temperature peak between 50°C and 200°C is associated with the non-evaporative water in cement samples and the weak volatiles of bound water in AFt and C–S–H gel. The weight loss between 400°C~500°C corresponds to the thermal decomposition and dehydration of $Ca(OH)_2$. The peak in the temperature range of 650°C~850°C is assigned to the thermal decomposition of calcium carbonate, which was produced by the carbonization during the long-term curing and preparation of cement samples [36]. Each component in the TG curve is similar to the weight loss features of ordinary Portland cement. This indicates that the incorporation of GM did not change the type of hydration products of the cement. GM-1, GM-2, and GM-3 had higher weight-loss rates in the first 3 d age with respect to the M18-0 sample, suggesting that GM promotes cement hydration in the early hydration stage. After 3 d of aging, the highest weight loss rate was achieved from the GM-2 sample, demonstrating that GM-2 had the highest hydration degree with the strongest hydration promotion effect on cement.

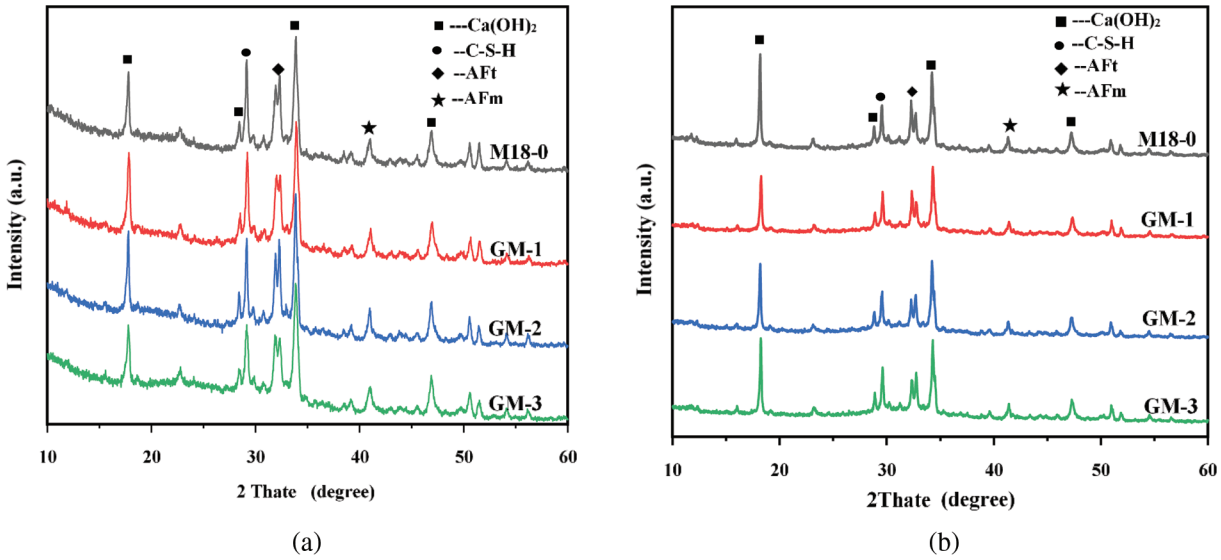

Figure 6: XRD spectra of GM/cement hardened slurry: (a) 3 d; (b) 28 d

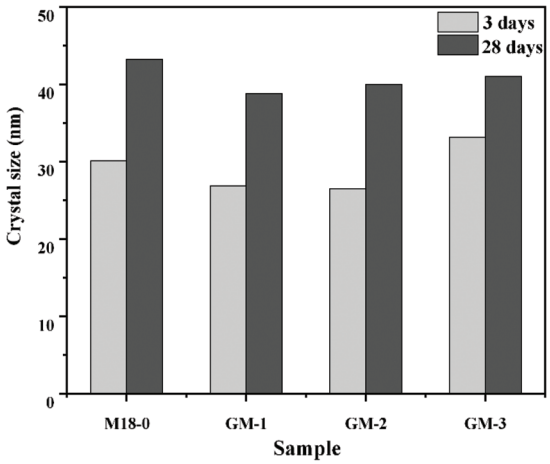

Figure 7: Effect of GM on the microcrystal size of the hydration product $Ca(OH)_2$ [0 0 1]

Fig. 9 shows the content of $Ca(OH)_2$ calculated by TG curve and formula (4) for each component at 3 d and 28 d age. Compared to the M18-0 group, the $Ca(OH)_2$ content of the GM component samples increased after 3 d of maintenance, by 1.23%, 2.56%, and 2.21% for GM-1, GM-2, and GM-3, respectively. This indicated that GM accelerates the early hydration of the cement and improves the hydration process. Since the effect of GO on $Ca(OH)_2$ crystallization is mainly at the early stage of cement hydration, the $Ca(OH)_2$ contents of the GM component samples and M18-0 sample are significantly different after curing for 3 d, which is consistent with the thermal analysis results for the hydration process. After 28 d of curing, the M18-0 group samples continued to hydrate represented by a larger increase in $Ca(OH)_2$ content. However, for the GM group, the increase of $Ca(OH)_2$ between 3 d and 28 d was insignificant due to the initial fast hydration promoted by the GO. At 28 d, the $Ca(OH)_2$ content of the GM experimental group was similar to that of M18-0.

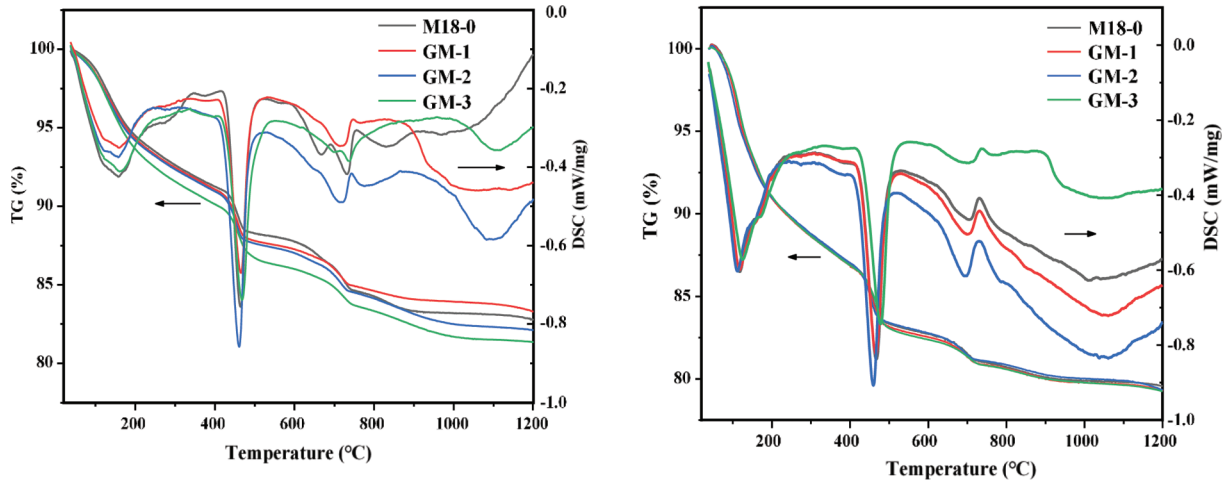

Figure 8: TG/DSC curves of GM/cement: (a) 3 d and (b) 28 d

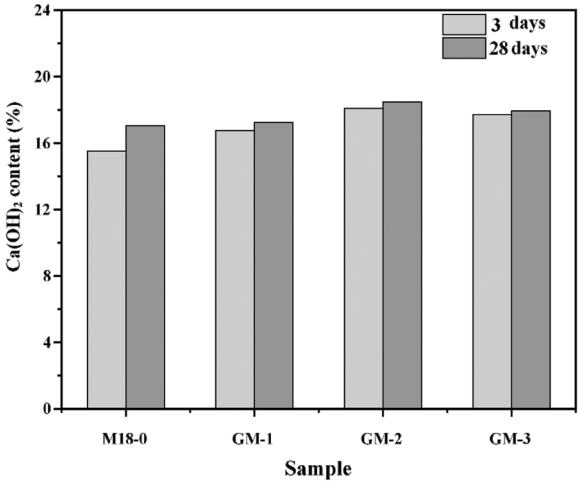

Figure 9: Effect of GM on $Ca(OH)_2$ content

3.5 Effect of GM on Pore Structure and Micromorphology of Cement Composites

The pore structure is an important part of the micromorphology of cement composites, which has an important influence on the working properties and durability of cement-based materials. Different pore sizes have a greater impact on the performance of cement. It has been suggested that pores can be classified into four classes: pores less than 20 nm in diameter are non-hazardous pores, in which water is bound to hydration products and cannot migrate. Pore sizes between 20 and 50 nm are less harmful pores, while between 50 and 200 nm, the pores are harmful, and pores larger than 200 nm are more harmful pores [37]. For large pores, the evaporation of free water leaves large cavities that can reduce the strength of the substrate [38,39]. MIP is a common method for characterizing the structure of porous materials. In this study, the change in pore size distribution and porosity of the cement at 3 d and 28 d of hydration was examined by MIP. Fig. 10 shows the pore structure parameters of the hardened cement slurry measured by MIP. After 3 d of aging, the total porosity of M18-0, GM-1, GM-2, and GM-3 was 16.29%, 16.01%, 15.90%, and 18.00%, respectively. GM-1 and GM-2 had the lowest porosity than that

of the M18-0 group. GM-3 group had the highest content of GO, which led to a decrease in the fluidity of cement. The cement matrix was poorly formed and the residual air bubbles produced pores in the hardened cement slurry, resulting in a higher total porosity than the M18-0 group. After curing for 28 d, the total porosity of each component had little difference, but the harmless pores (<20 nm) and less harmful pores (20–50 nm) in the GM-1, GM-2, and GM-3 were higher than those in the M18-0 Group. This means that the GM has an optimizing effect on the pore structure. Cement dissolves immediately after contact with water. When the hydration reaction occurs, the volume of hydration products increases. They fill the voids between the cement particles which were initially occupied by free water. The promoted nucleation of the hydration products by GO can accelerate the hydration of the cement and increase the volume of the hydration products to fill more space. Fig. 11 shows the SEM pictures of the cement slurry after hardening and curing for 28 d. As seen from the SEM images, the microstructure of the M18-0 sample is mainly disordered and loosely packed containing large pores between crystals. The cement hydration crystals in the GM groups are much more compact with significantly reduced density of microscopic cavities due to the accelerated hydration by the addition of GO to form a dense hydration product. The reduced microporosity helps to hinder the crack expansion, which improves the strength and durability of the cement.

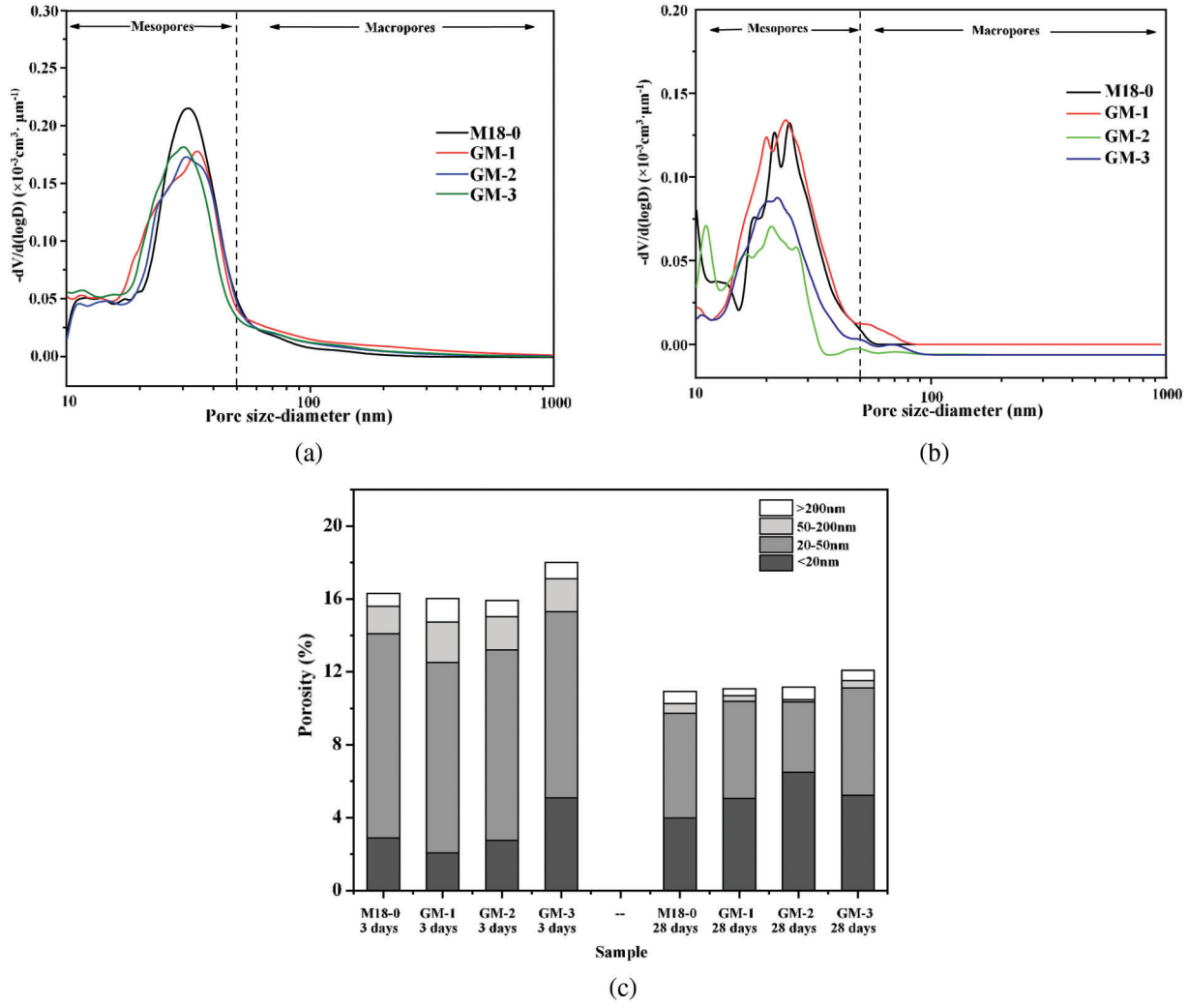

Figure 10: Pore size distribution and porosity of GM/cement composites: (a) 3 d; (b) 28 d and (c) porosity

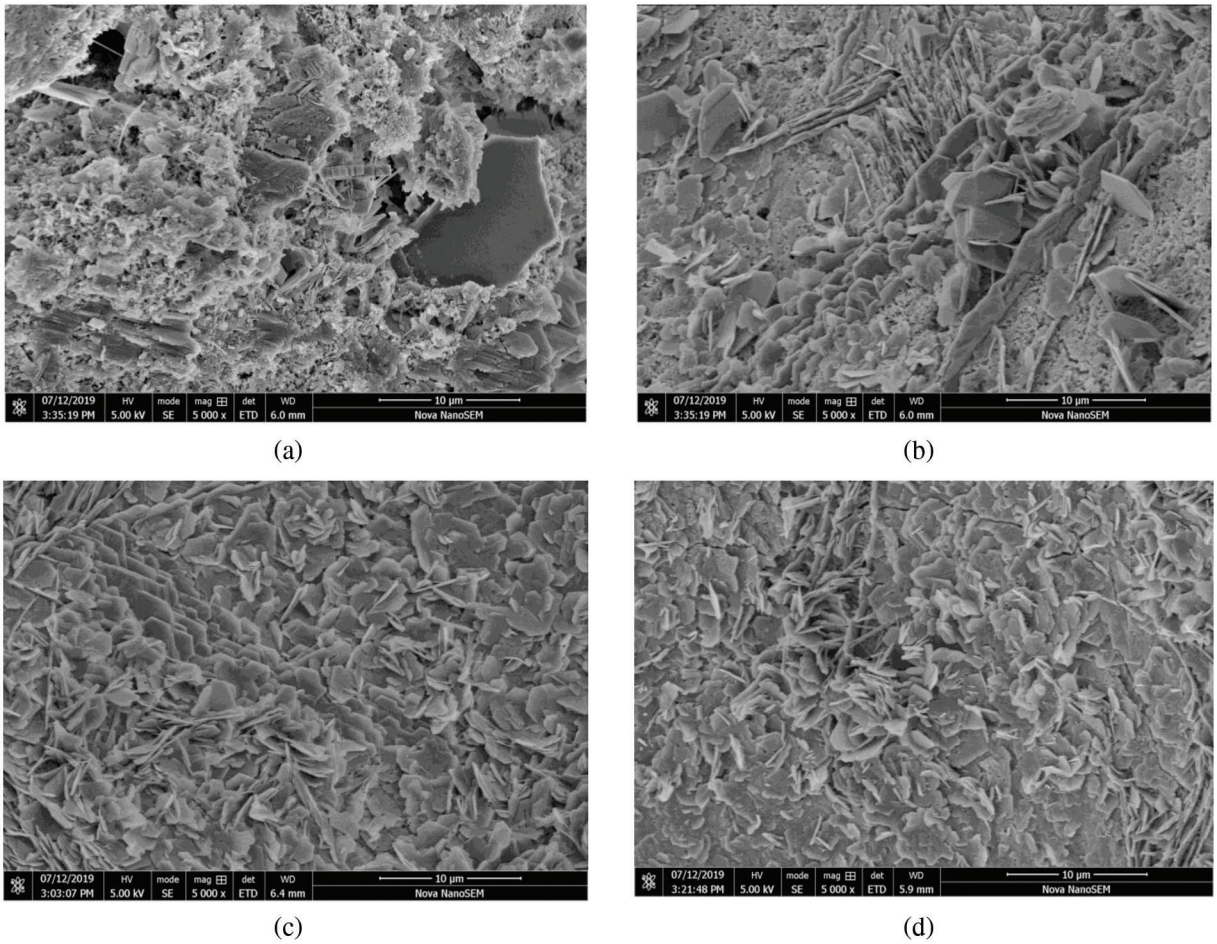

Figure 11: SEM pictures of cement after curing at 28 d (a) M18-0; (b) GM-1; (c) GM-2 and (d) GM-3

3.6 Effect of GM on the Mechanical Properties of Cement-Based Materials

The results of the flexural and compressive strength tests of the cement mortar are displayed in Fig. 12. Compared to M18-0, the compressive and flexural strengths of the cement mortars in the GM-1 and GM-2 groups were increased. After 28 d, the compressive strength and the flexural strength of the GM-1 group were increased by 16.07% and 4.1%, respectively. Meanwhile, the compressive strength and the flexural strength of the GM-2 group were increased by 6.10% and 11.85%, respectively. The early strength of the GM-3 group is lower than that of M18-0. If the GO dose is too high, the cement strength was decreased. Since too much GO affected the flow of the cement, resulting in more air bubbles in the slurry, which is detrimental to the strength of the cement by the high density voids in the hardened cement slurry.

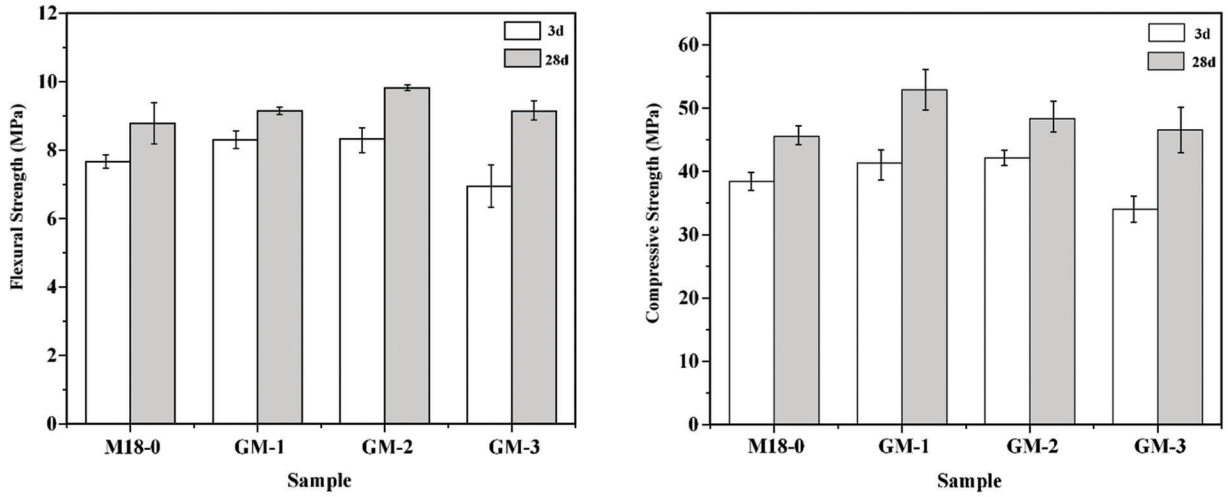

Figure 12: The influence of GM on mechanical properties of the cement mortar. (a) Flexural strength; (b) Compressive strength

4 Conclusions

In this study, GM compound superplasticizer was obtained by thermally blending GO and M18 polycarboxylate superplasticizer. The effects of GM on cement hydration rate, hydration properties, type and content of hydration products, microscopic pore structure, and mechanical properties are investigated. The method in this paper provides an idea for the preparation of high performance concrete which promotes construction materials continued development. The result is as follows:

1. The main forces between GO and M18 are hydrogen bonding and intermolecular forces. The long chain structure of M18 repels each other increasing the layer spacing of GO and weakening the force between GO sheets, thus enabling the GO sheets to be uniformly dispersed in the cement slurry.
2. GM does not directly participate in the hydration reaction of cement and change the type of hydration products. But it can promote the early hydration process of cement and obviously affect the crystallization state of $Ca(OH)_2$. GM increases the $Ca(OH)_2$ content with a decreased grain size, in which GM-1 and GM-2 have a more obvious effect.
3. GM can improve the micro pores of cement, refine the pore diameter and increase the proportion of harmless and less harmful pores. However, it affects the total porosity of cement to a lesser extent.
4. GM improves the mechanical properties of the cement stone. After 28 d, the flexural strength of GM-1 and GM-2 groups increased by 4.10%, 11.85% and compressive strength increased by 16.07% and 6.10%, respectively, compared to the M18-0 group.

Acknowledgement: The authors would like to acknowledge the assistance from Shun Zhou, Xiaotao Zhang and Jiawei Jiao from Nanjing Tech University.

Author Contributions: Writing—original draft, D.L.; Validation, S.Z.; Data curation, X.Z.; Writing—review & editing, validation, J.J. All authors have read and agreed to the published version of the manuscript.

Data Availability Statement: The data presented in this study are available on request from the corresponding author.

Funding Statement: This research was funded by the National Natural Science Foundation of China (No. 51872137) and Priority Academic Program Development of Jiangsu Higher Education Institutions (PAPD).

Conflicts of Interest: The authors declare that they have no conflicts of interest to report regarding the present study.

References

1. Stefanidou, M., Papayianni, I. (2012). Influence of nano-SiO on the Portland cement slurrys. *Composites Part B, 43(6),* 2706–2710. DOI 10.1016/j.compositesb.2011.12.015.
2. Nadiv, K., Shtein, M., Peled, A., Regev, O. (2015). WS_2 nanotube–Reinforced cement: Dispersion matters. *Construction & Building Materials, 98(15),* 112–118. DOI 10.1016/j.conbuildmat.2015.08.085.
3. Peng, H., Ge, Y., Cai, C. S., Zhang, Y., Liu, Z. et al. (2019). Mechanical properties and microstructure of graphene oxide cement-based composites. *Construction and Building Materials, 194(10),* 102–109. DOI 10.1016/j.conbuildmat.2018.10.234.
4. Mohsen, M. O., Taha, R., Taqa, A. A., Shaat, A. (2017). Optimum carbon nanotubes' content for improving flexural and compressive strength of cement slurry. *Construction & Building Materials, 150(19),* 395–403. DOI 10.1016/j.conbuildmat.2021.124850.
5. Onaizi, A. M., Huseien, F. G., Lim, N. H., Amran, M., Mostafa, S. (2021). Effect of nanomaterials inclusion on sustainability of cement-based concretes: A comprehensive review. *Construction and Building Materials, 306(1),* 124850. DOI 10.1515/ntrev-2020-0011.
6. Du, M. R., Jing, H. W., Gao, Y., Su, H. J., Fang, H. Y. et al. (2020). Carbon nanomaterials enhanced cement-based composites: Advances and challenges. *Nanotechnology Reviews, 9,* 115–135. DOI 10.1016/j.conbuildmat.2017.06.020.
7. Nadiv, R., Shtein, M., Refaeli, M., Peled, A., Regev, O. et al. (2016). The critical role of nanotube shape in cement composites. *Cement & Concrete Composites, 71(6119),* 166–174. DOI 10.1016/j.cemconcomp.2016.05.012.
8. Sheikh, T. M., Anwar, M. P., Muthoosamy, K., Jaganathan, J., Chan, A. et al. (2021). The mechanics of carbon-based nanomaterials as cement reinforcement—A critical review. *Construction & Building Materials, 303(17),* 124441. DOI 10.1016/j.conbuildmat.2021.124441.
9. Asgari, H., Ramezanianpour, A., Butt, H. J. (2016). Effect of water and nano-silica solution on the early stages cement hydration. *Construction and Building Materials, 129(4),* 11–24. DOI 10.1016/j.conbuildmat.2016.11.009.
10. Shao, G., Lu, Y., Wu, F., Yang, C., Zeng, F. et al. (2012). Graphene oxide: the mechanisms of oxidation and exfoliation. *Journal of Materials Science, 47(10),* 4400–4409. DOI 10.1007/s10853-012-6294-5.
11. Dreyer, D. R., Park, S., Bielawski, C. W., Ruoff, R. S. (2009). The chemistry of graphene oxide. *Chemical Society Reviews, 39(1),* 228–240. DOI 10.1039/b917103g.
12. Wang, Q., Li, S., Pan, S., Cui, X., Corr, D. J. et al. (2019). Effect of graphene oxide on the hydration and microstructure of fly ash-cement system. *Construction and Building Materials, 198(20),* 106–119. DOI 10.1016/j.conbuildmat.2018.11.199.
13. Wang, Y., Yang, J., Ouyang, D. (2019). Effect of graphene oxide on mechanical properties of cement mortar and its strengthening mechanism. *Materials, 12(22),* 3753. DOI 10.3390/ma12223753.
14. Qiao, M., Shan, G., Chen, J., Wu, S. S., Gao, N. X. et al. (2020). Effects of salts and adsorption on the performance of air entraining agent with different charge type in solution and cement mortar. *Construction and Building Materials, 242,* 118188. DOI 10.1016/j.conbuildmat.2020.118188.
15. Devi, S. C., Khan, R. A. (2020). Compressive strength and durability behavior of graphene oxide reinforced concrete composites containing recycled concrete aggregate. *Journal of Building Engineering, 32,* 101800. DOI 10.1016/j.jobe.2020.101800.
16. An, J., Nam, B. H., Alharbi, Y., Hooi, B. (2019). Edge-oxidized graphene oxide (EOGO) in cement composites: Cement hydration and microstructure. *Composites, 173(15),* 106795.1–106795.12. DOI 10.1016/j.compositesb.2019.05.006.
17. Chuah, S., Li, W. G., Chen, S. J., Sanjayan, J. G., Duan, W. H. (2018). Investigation on dispersion of graphene oxide in cement composite using different surfactant treatments. *Construction & Building Materials, 161(9),* 519–527. DOI 10.1016/j.conbuildmat.2017.11.154.

18. Li, X., Wang, L., Liu, Y., Li, W., Wen, H. D. (2018). Dispersion of graphene oxide agglomerates in cement slurry and its effects on electrical resistivity and flexural strength. *Cement and Concrete Composites, 92(122),* 145–154. DOI 10.1016/j.cemconcomp.2018.06.008.
19. Rahul, R., Ananda, M., Ganesh, A. T., Sairam, V. (2018). Effect of Graphene Oxide Nanosheets dispersion in cement mortar composites incorporating Metakaolin and Silica Fume. *Construction and Building Materials, 186(4),* 514–524. DOI 10.1016/j.conbuildmat.2018.07.135.
20. Ma, P. C., Siddiqui, N. A., Marom, G., Kim, J. K. (2010). Dispersion and functionalization of carbon nanotubes for polymer-based nanocomposites: A review. *Composites Part A: Applied Science and Manufacturing, 41(10),* 1345–1367. DOI 10.1016/j.compositesa.2010.07.003.
21. Strano, M. S., Moore, V. C., Miller, M. K., Allen, M. J., Haroz, E. H. et al. (2003). The role of surfactant adsorption during ultrasonication in the dispersion of single-walled carbon nanotubes. *Journal of Nanoscience and Nanotechnology, 3(1),* 81–86. DOI 10.1166/jnn.2003.194.
22. Yavari, N., Poorabdollah, M., Rajabi, L. (2021). Graphene oxide and silane-modified graphene oxide/unsaturated polyester resin nanocomposites: A comparative cure kinetic and diffusion study. *Thermochimica Acta, 707,* 179081. DOI 10.1016/j.tca.2021.179081.
23. Zhang, X. T., Zhou, S., Zhou, H., Li, D. X. (2022). The effect of the modification of graphene oxide with γ-aminopropyltriethoxysilane (KH550) on the properties and hydration of cement. *Construction and Building Materials, 322(18),* 126497. DOI 10.1016/j.conbuildmat.2022.126497.
24. Pooneh, H., Mehdi, G., Bahram, R., Ghasem, B., Mohammad, R. S. (2019). Polyurethane coatings reinforced with 3-(triethoxysilyl)propyl isocyanate functionalized graphene oxide nanosheets: Mechanical and anti-corrosion properties. *Progress in Organic Coatings, 136,* 105243. DOI 10.1016/j.porgcoat.2019.105243.
25. Xun, W. J., Wu, C. L., Li, J. Y., Yang, C. W., Li, Y. (2020). Effect of functional polycarboxylic acid superplasticizers on mechanical and rheological properties of cement slurry and mortar. *Applied Sciences, 10(16),* 5418. DOI 10.3390/app10165418.
26. Zhang, J., Ma, Y. F., Wang, J., Gao, N. X., Hu, Z. L. et al. (2022). A novel shrinkage-reducing polycarboxylate superplasticizer for cement-based materials: Synthesis, performance and mechanisms. *Construction and Building Materials, 321(2),* 321126342. DOI 10.1016/j.conbuildmat.2022.126342.
27. Li, X. Y., Korayem, A. H., Li, C. Y., Liu, Y. M., He, H. S. et al. (2016). Incorporation of graphene oxide and silica fume into cement slurry: A study of dispersion and compressive strength. *Construction and Building Materials, 123(7100),* 327–335. DOI 10.1016/j.conbuildmat.2016.07.022.
28. Li, X., Lu, Z., Chuah, S., Li, W., Liu, Y. et al. (2017). Effects of graphene oxide aggregates on hydration degree, sorptivity, and tensile splitting strength of cement slurry. *Composites Part A: Applied Science and Manufacturing, 100,* 1–8. DOI 10.1016/j.compositesa.2017.05.002.
29. Liu, M., Lei, J., Guo, L., Du, X., Li, J. (2015). The application of thermal analysis, XRD and SEM to study the hydration behavior of tricalcium silicate in the presence of a polycarboxylate superplasticizer. *Thermochimica Acta, 613,* 54–60. DOI 10.1016/j.tca.2015.05.020.
30. Esteves, L. P. (2011). On the hydration of water-entrained cement-silica systems: Combined SEM, XRD and thermal analysis in cement slurrys. *Thermochimica Acta, 518(1),* 27–35. DOI 10.1016/j.tca.2011.02.003.
31. Wu, L., Liu, L., Gao, B., Rafael, M. C., Zhang, M. et al. (2013). Aggregation kinetics of graphene oxides in aqueous solutions: Experiments, mechanisms, and modeling. *Langmuir, 29(49),* 15174–15181. DOI 10.1021/la404134x.
32. Anagnostopoulos, C. A. (2014). Effect of different superplasticisers on the physical and mechanical properties of cement grouts. *Construction and Building Materials, 50(4),* 162–168. DOI 10.1016/j.conbuildmat.2013.09.050.
33. Mohammed, A., Alsaadi, N., Almahaidi, R. (2017). Utilization of graphene oxide to synthesize high-strength cement-based adhesive. *Journal of Materials in Civil Engineering, 29(4),* 4016258.1–4016258.7. DOI 10.1061/(ASCE)MT.1943-5533.0001705.
34. Scrivener, K. L., Juilland, P., Monteiro, P. (2015). Advances in understanding hydration of portland cement. *Cement & Concrete Research, 78(10),* 38–56. DOI 10.1016/j.cemconres.2015.05.025.

35. Schwyzer, I., Kaegi, R., Sigg, L., Nowack, B. (2013). Colloidal stability of suspended and agglomerate structures of settled carbon nanotubes in different aqueous matrices. *Water Research, 47(12),* 3910–3920. DOI 10.1016/j.watres.2013.01.057.
36. Luo, X., Fan, W., Li, C., Wang, Y., Yangm, S. (2020). Effect of hydroxyacetic acid on the water resistance of magnesium oxychloride cement. *Construction and Building Materials, 246(6),* 118428. DOI 10.1016/j.conbuildmat.2020.118428.
37. Wang, M., Wang, R., Yao, H., Farhan, S., Zheng, S. et al. (2016). Study on the three dimensional mechanism of graphene oxide nanosheets modified cement. *Construction and Building Materials, 126(15),* 730–739. DOI 10.1016/j.conbuildmat.2016.09.092.
38. Li, H. X., Xue, Z., Liang, H., Guo, Y. C., Liang, G. W. et al. (2021). Influence of defoaming agents on mechanical performances and pore characteristics of portland cement paste/mortar in presence of EVA dispersible powder. *Journal of Building Engineering, 41(5),* 102780. DOI 10.1016/j.jobe.2021.102780.
39. Wang, Y. L., He, F. X., Wang, J. J., Wang, C., Xiong, Z. Q. (2019). Effects of calcium bicarbonate on the properties of ordinary Portland cement paste. *Construction and Building Materials, 225(20),* 591–600. DOI 10.1016/j.conbuildmat.2019.07.262.